NANO MICRO small

Supporting Information

for *Small,* DOI: 10.1002/smll.202207080

Highly Crystalline Prussian Blue for Kinetics Enhanced Potassium Storage

Wenli Shu, Meng Huang, Lishan Geng, Fan Qiao, and Xuanpeng Wang**

Supporting Information

Highly Crystalline Prussian Blue for Kinetics Enhanced Potassium Storage

Wenli Shu, Meng Huang, Lishan Geng, Fan Qiao, and Xuanpeng Wang**

W. Shu, M. Huang, L. Geng, F. Qiao, X. Wang
School of Materials Science and Engineering, Hainan Institute, Wuhan University of Technology, Wuhan 430070, P.R. China
E-mail: 211808@whut.edu.cn
W. Shu, M. Huang, X. Wang
Hainan Institute, Wuhan University of Technology, Sanya 572000, China
X. Wang
Hubei Longzhong Laboratory, Wuhan University of Technology (Xiangyang Demonstration Zone), Xiangyang 441000, P.R. China
X. Wang
Department of Physical Science & Technology, School of Science, Wuhan University of Technology, Wuhan 430070, P.R. China
E-mail: wxp122525691@whut.edu.cn

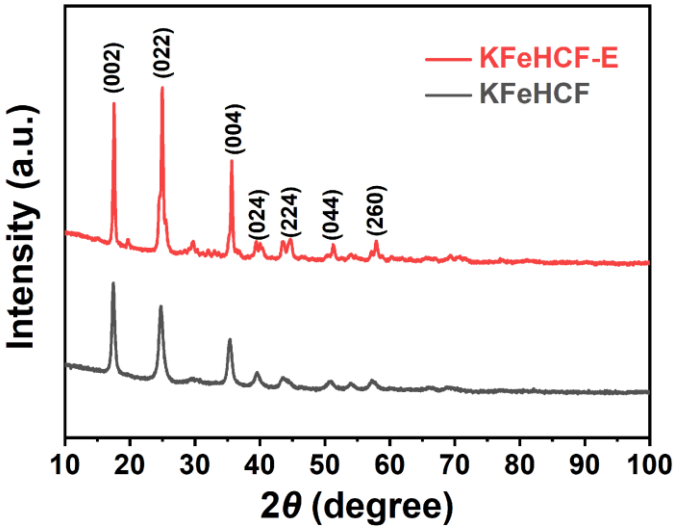

Figure S1. XRD patterns of KFeHCF-E and KFeHCF.

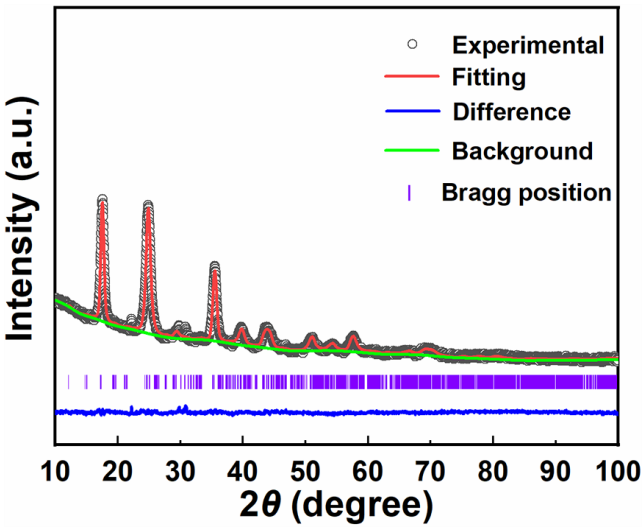

Figure S2. Rietveld refinement XRD pattern of KFeHCF.

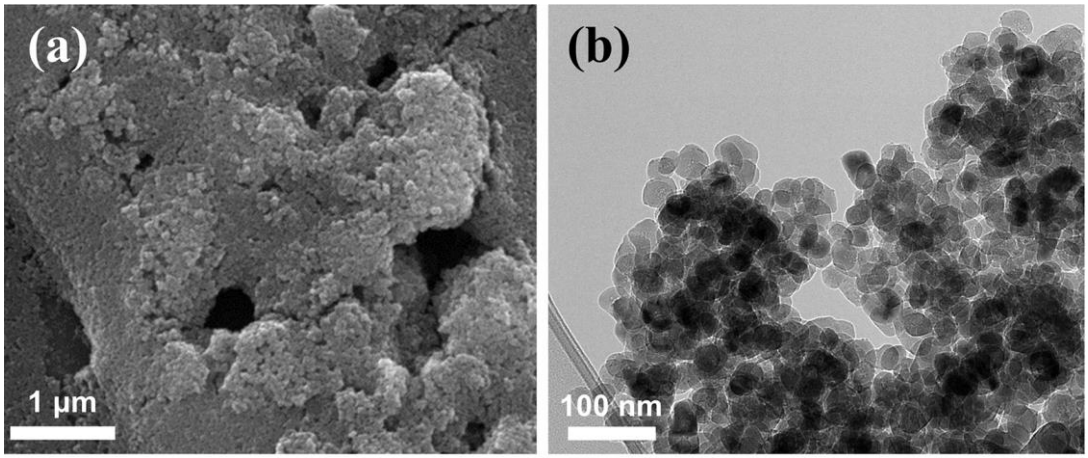

Figure S3. (a) SEM and (b) TEM image of KFeHCF-E.

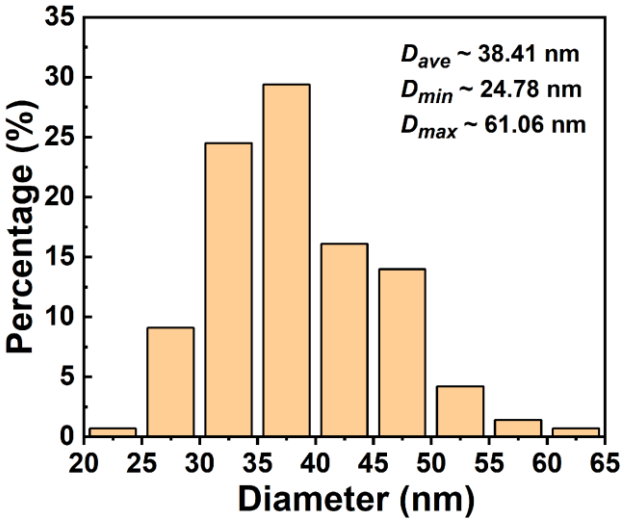

Figure S4. The size distribution of KFeHCF-E, counted and calculated from Figure S3b.

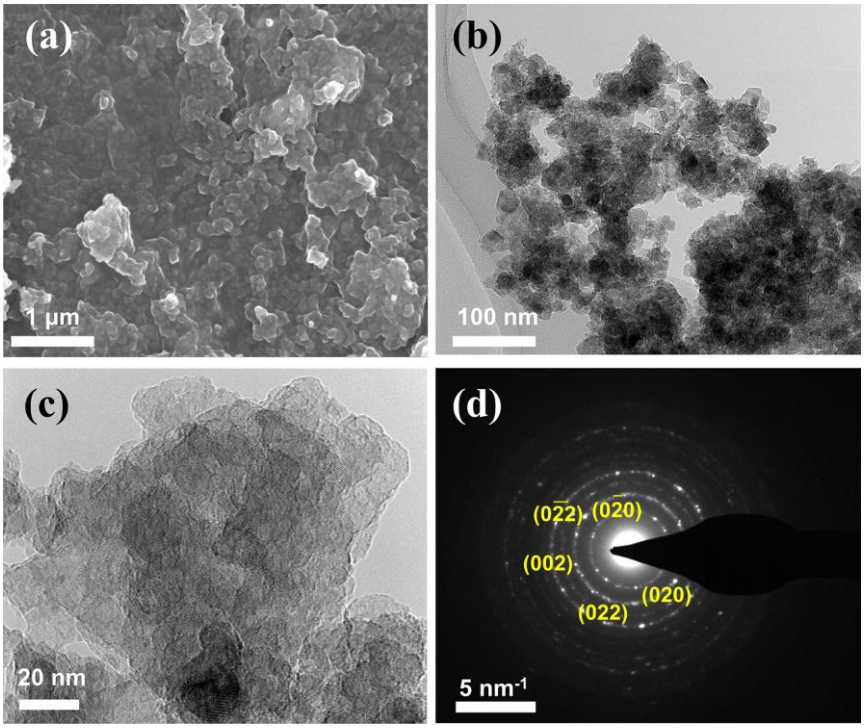

Figure S5. Characterizations of KFeHCF: (a) SEM image. (b-d) TEM images and SAED pattern.

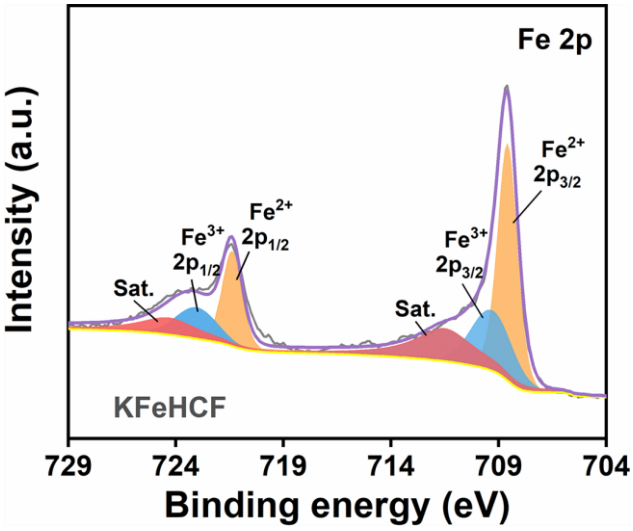

Figure S6. Fe 2p fitting spectra of KFeHCF.

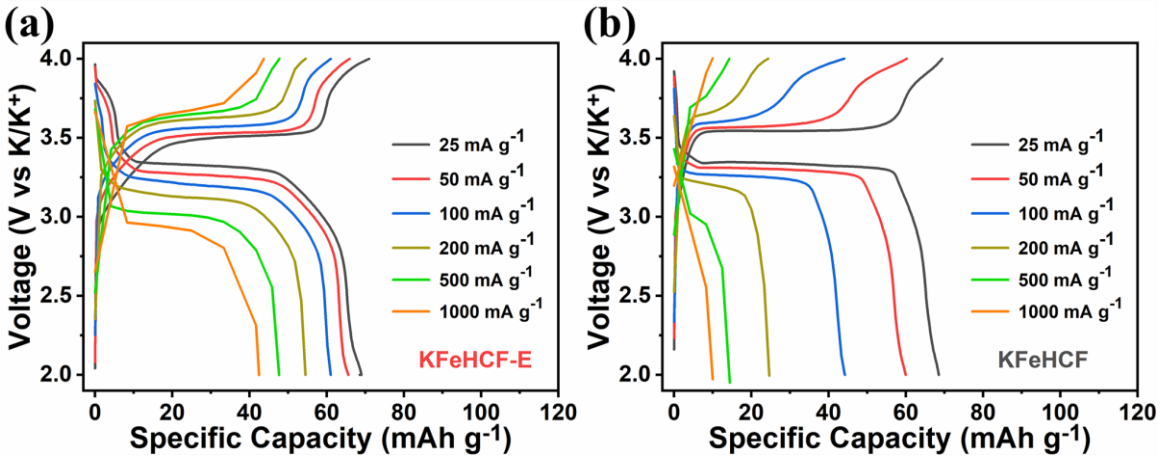

Figure S7. Charge/discharge profiles at various current densities of (a) KFeHCF-E and (b) KFeHCF.

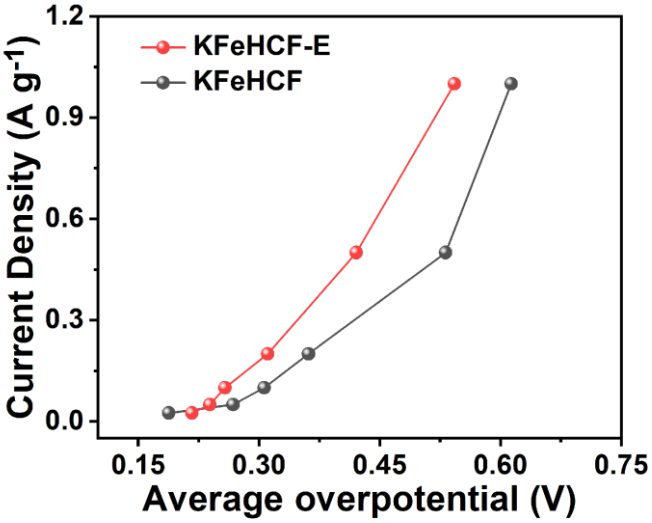

Figure S8. Derived plots of average overpotential *vs.* current density.

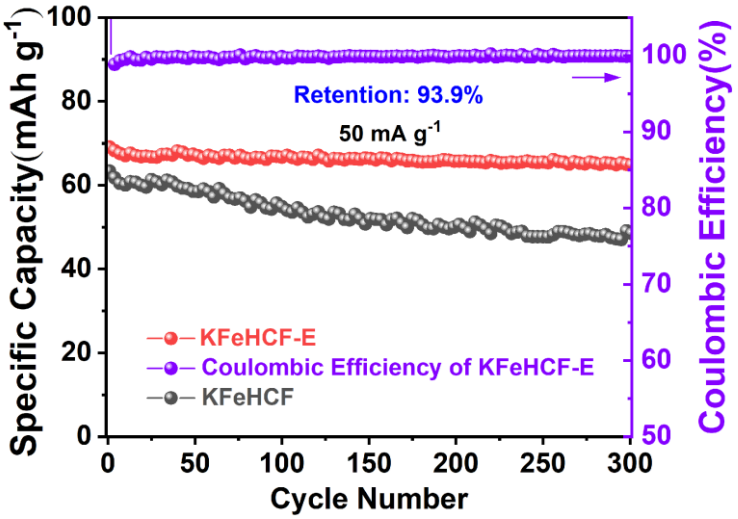

Figure S9. Cycling comparison performance at 50 mA g^{-1}.

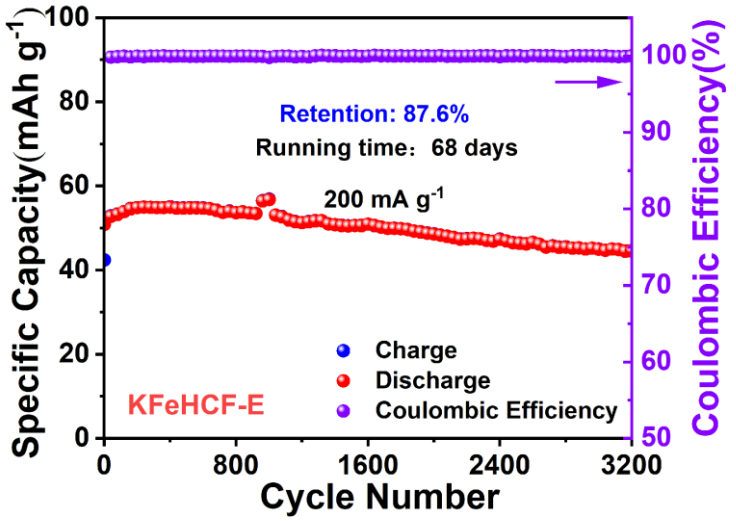

Figure S10. Long-term cycle performance of KFeHCF-E at 200 mA g^{-1}.

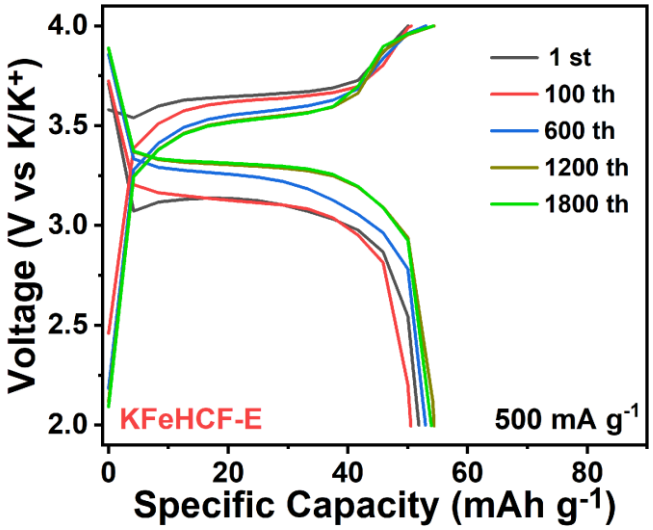

Figure S11. Charge/discharge profiles of KFeHCF-E at 500 mA g^{-1}.

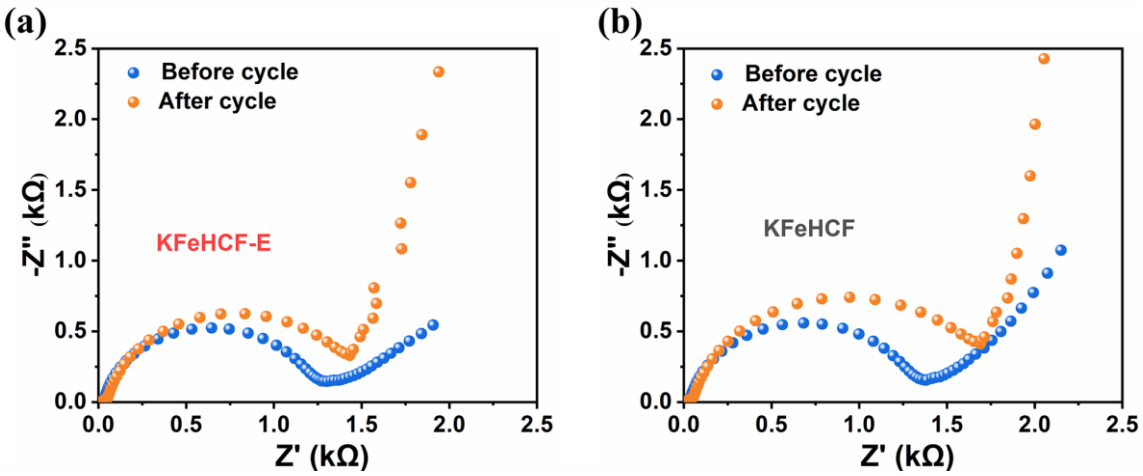

Figure S12. EIS of (a) KFeHCF-E and (b) KFeHCF.

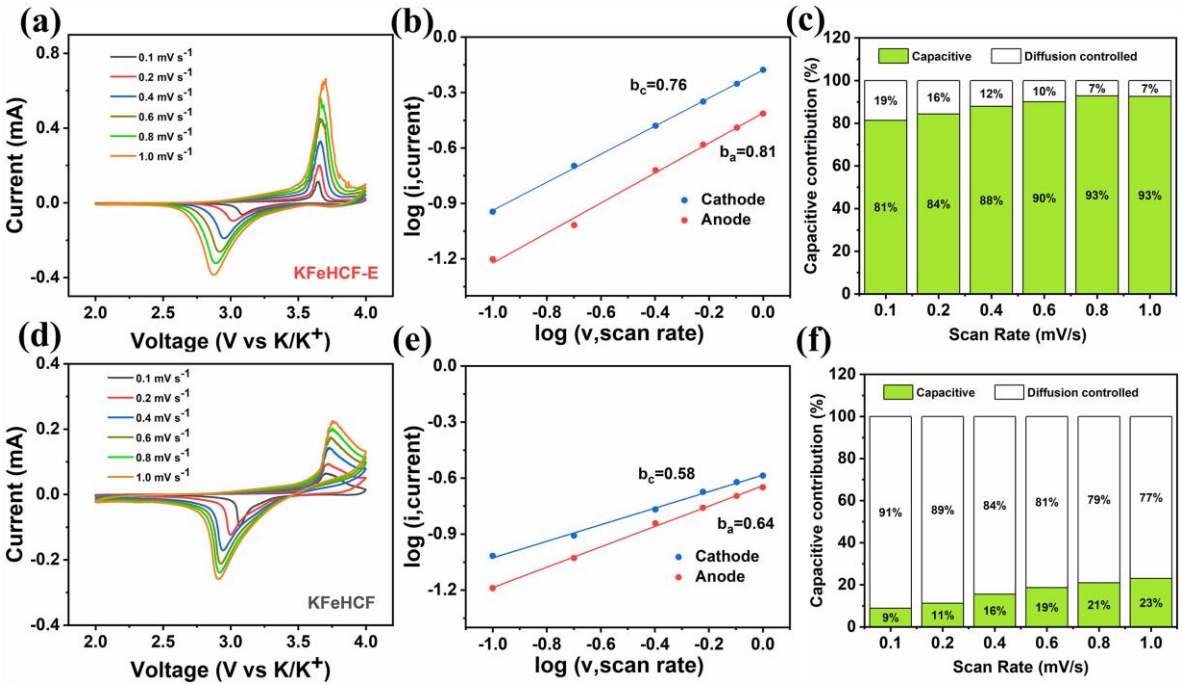

Figure S13. CV curves of KFeHCF-E (a)and KFeHCF (d) at scan rates range from 0.1 to1.0 mV s^{-1}. Linear relationship of log(i) vs. log(v) of KFeHCF-E (b) and KFeHCF (e). The percentage of capacitive and diffusion-controlled contributions for KFeHCF-E (c) and KFeHCF (f) at various scan rates.

Scheme 1. A general method to measure the degree of pseudocapacitive effect is to make a qualitative analysis based on the following equation: $i = av^b$, where a and b are constants.[1] Generally, for the ideal Faraday intercalation process controlled by the diffusion effect, the b value is 0.5; for a surface-dominated process without diffusion control, the b value is 1.0.[2] Moreover, by further dividing the response current at the same potential into a surface-dominated process ($k_1 v$) and a diffusion-dependent process ($k_2 v^{1/2}$) as the following equation: $i = k_1 v + k_2 v^{1/2}$, the percentage of capacitive contribution can be quantified.

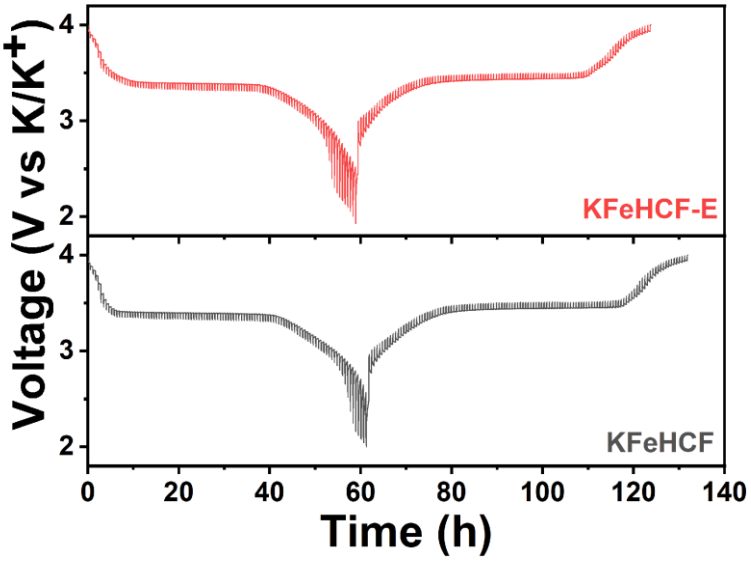

Figure S14. GITT curves of the initial discharge/charge process at 8 mA g^{-1}.

Scheme 2. The diffusion coefficient of K^+ is calculated[3]:

$$D = \frac{4}{\pi\tau}\left(\frac{m_B V_M}{M_B S}\right)^2 \left(\frac{\Delta E_S}{\Delta E_\tau}\right)^2$$

Where τ refers to constant current pulse time, m_B, V_M, M_B, and S are the mass, molar volume, molar mass of the cathode material, and electrode-electrolyte interface area, respectively. $\triangle E_S$ is voltage difference during a single-step experiment, and $\triangle E_\tau$ is the total change of cell voltage during a constant current pulse excluding the IR drop.

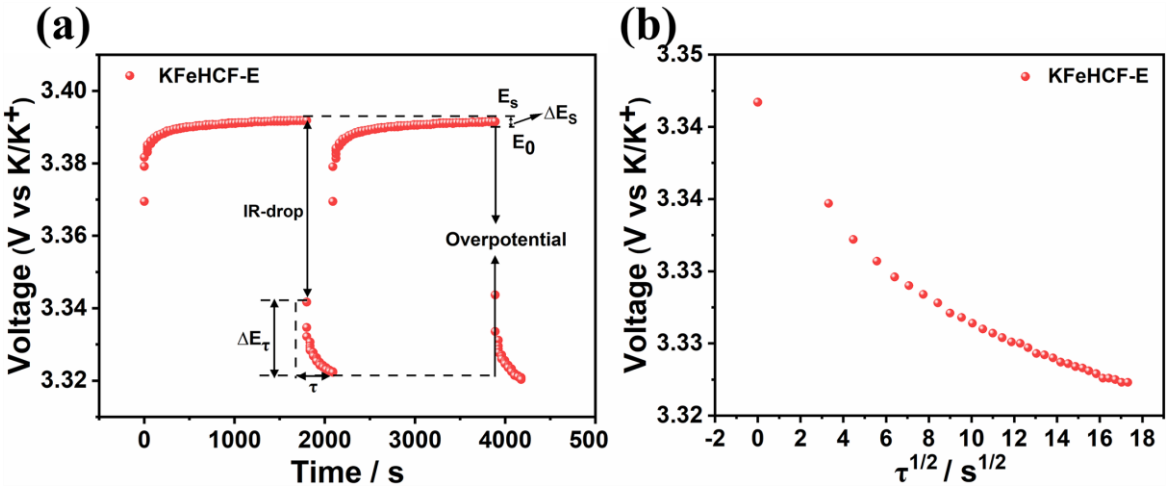

Figure S15. (a) The two pulse-relaxation cycles at DOC of ~40%, and (b) the plots of voltage as a function of $\tau^{1/2}$ of single discharge process of KFeHCF-E.

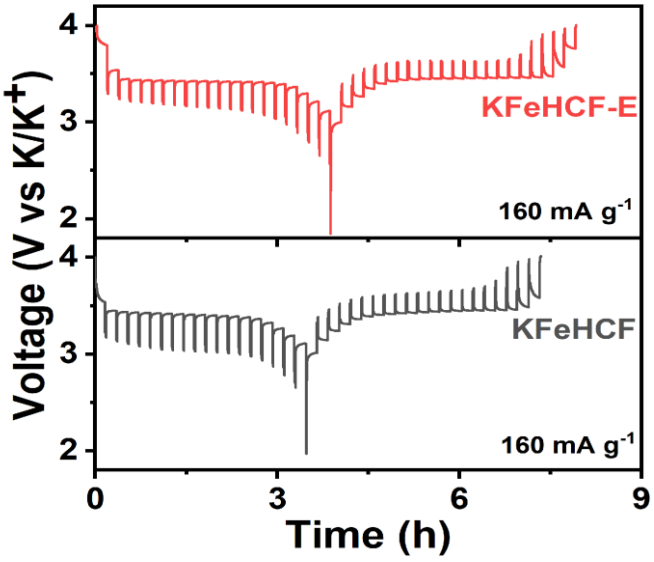

Figure S16. GITT potential response curve with time. The experiment was conducted at constant current pulse of 160 mA g^{-1} for 1 min followed by a relaxation period of 10 min.

Table S1. ICP and elemental analysis results of KFeHCF-E and KFeHCF.

Sample	K content	Fe content	C content	N content
KFeHCF-E	0.859	1	3.126	2.801
KFeHCF	0.823	1	3.073	2.710

Scheme 3. The general molecular formulae of Prussian blue is $K_xFe[Fe(CN)_6]_y \cdot zH_2O$. The molar ratio of cyanide in the samples is calculated based on the molar ratio of N.[4]

For the KFeHCF-E, the detailed calculation process is given as follows:

$$\frac{x}{1+y} = 0.859$$

$$\frac{6y}{1+y} = 2.801$$

$$\frac{18z}{39x + 56(1+y) + 156y} = 0.0283$$

Calculated: x=1.61; y=0.88; z=0.43

For KFeHCF:

$$\frac{x}{1+y} = 0.823$$

$$\frac{6y}{1+y} = 2.710$$

$$\frac{18z}{39x + 56(1+y) + 156y} = 0.0403$$

Calculated: x=1.51; y=0.82; z=0.59

Thus, the molecular formulaes of KFeHCF-E and KFeHCF are $K_{1.61}Fe[Fe(CN)_6]_{0.88}\cdot 0.43H_2O$ and $K_{1.51}Fe[Fe(CN)_6]_{0.82}\cdot 0.59H_2O$, respectively.

Table S2. Structural parameters of KFeHCF-E obtained from Rietveld analysis.

Atom	Wyckoff	x	y	z	Occupancy
K1	4e	0.2647(30)	0.2772(22)	0.2266(22)	0.84771
K2	4e	0.2363(11)	0.7309(10)	0.2649(13)	0.93234
Fe1	2a	0	0	0	1
Fe2	2d	0.5	0	0.5	1
Fe3	2b	0.5	0	0	1
Fe4	2c	0	0	0.5	1
C1	4e	0.183(8)	0.014(17)	0.018(11)	1
C2	4e	0.03100	0.18000	0.01500	0.99041
C3	4e	0.00700	-0.00800	0.18700	1
C4	4e	0.52700	0.52700	0.17300	1
C5	4e	0.50600	0.17900	0.50400	1
C6	4e	0.68400	0.47900	0.02500	1
N1	4e	0.2890(22)	0.006(6)	0.0280(28)	1
N2	4e	0.02800	0.28600	0.06100	0.99041
N3	4e	-0.01100	0.06200	0.27600	1
N4	4e	0.50400	0.50200	0.0280(28)	1
N5	4e	0.52800	0.28900	0.52200	1
N6	4e	0.78900	0.51400	0.00300	1
O1	4e	0.265(18)	0.265(17)	0.229(15)	0.15224
O2	4e	0.223(27)	0.73(4)	0.301(25)	0.06768

S.G. $P2_1/n$ a = 10.0652(4), b = 10.0754(5), c = 10.0298(9) Å, α=γ=90° β= 92.216(8)°
R_p = 0.99%, R_{wp} = 1.41%, Chi2= 4.44

Table S3. Structural parameters of KFeHCF obtained from Rietveld analysis.

Atom	Wyckoff	x	y	z	Occupancy
K1	4e	0.24738	0.27483	0.24656	0.60994
K2	4e	0.24215	0.26764	0.25306	0.84474
Fe1	2a	0	0	0	1
Fe2	2d	0.5	0	0.5	1
Fe3	2b	0.5	0	0	1
Fe4	2c	0	0	0.5	1
C1	4e	0.19143	0.00748	0.05093	0.98387
C2	4e	-0.00731	0.17929	-0.01793	0.94983
C3	4e	0.00744	-0.02023	0.18833	0.9968
C4	4e	0.52444	0.48635	0.16590	1
C5	4e	0.48711	0.17790	0.48746	1
C6	4e	0.69610	0.48737	0.05009	1
N1	4e	0.29962	-0.00517	0.03812	0.98387
N2	4e	0.03508	0.26864	0.04330	0.94983
N3	4e	-0.00795	0.00511	0.29540	0.9968
N4	4e	0.48273	0.49744	0.28958	1
N5	4e	0.53099	0.28611	0.52642	1
N6	4e	0.79733	0.50117	0.03217	1
O1	4e	0.24913	0.26764	0.24623	0.39003
O2	4e	0.23917	0.72498	0.33236	0.15522
S.G. $P2_1/n$ a = 10.1070(7), b = 10.1261(8), c = 10.0810(15) Å, α=γ=90° β= 91.606(16)°					

R_p = 0.65%, R_{wp} = 0.83%, Chi2= 1.49

Table S4. Summary of KFeHCF-E or other cathodes for potassium-ion batteries.

Materials	Half-cell				References
	Average Voltage (V)	Capacity (mAh g^{-1})	Rate performance	Capacity retention	
KFeHCF-E	**3.4**	**77.0 (25 mA g^{-1})**	**42.5 (1 A g^{-1})**	**61.3% cycle 5000 (100 mA g^{-1})**	**This work**
KFeHCF-V	3.4	77.6 (25 mA g^{-1})	45.0 (200 mA g^{-1})	57.5% cycle 250 (100 mA g^{-1})	[5]
KPB-2E	3.35	70.9 (30 mA g^{-1})	44.5 (200 mA g^{-1})		[6]
$K_{0.220}Fe[Fe(CN)_6]_{0.805} \cdot 4.01H_2O$	3.3	74.5 (50 mA g^{-1})	36.0 (400 mA g^{-1})	86.5% cycle 150 (200 mA g^{-1})	[7]
$K_{1.4}Fe_4[Fe(CN)_6]_3$	3.2	71.0 (50 mA g^{-1})	24.9 (600 mA g^{-1})	75.2% cycle 100 (200 mA g^{-1})	[8]
$K_4Fe(CN)_6$/C	3.6	65.5 (20 mA g^{-1})	25.2 (200 mA g^{-1})	75.0% cycle 400 (20 mA g^{-1})	[9]
P3 - $K_{0.5}MnO_2$	2.6	100 (50 mA g^{-1})	72.0 (100 mA g^{-1})	86.5% cycle 150 (200 mA g^{-1})	[10]
K-birnessite $K_{0.77}MnO_2 \cdot 0.23H_2O$	2.75	134 (100 mA g^{-1})	77.0 (1 A g^{-1})	80.5% cycle 1000 (1 A g^{-1})	[11]
$KVOPO_4$	3.65	115 (24 mA g^{-1})	83.4 (2.4 A g^{-1})	86.8% cycle 100 (60 mA g^{-1})	[12]

References

[1] D. Chao, P. Liang, Z. Chen, L. Bai, H. Shen, X. Liu, X. Xia, Y. Zhao, SV Savilov, J. Lin, ZX. Shen, *ACS Nano* **2016**, *10*, 10211.

[2] Y. Xu, C. Zhang, M. Zhou, Q. Fu, C. Zhao, M. Wu, Y. Le, *Nat. Commun.* **2018**, *9*, 1720.

[3] W. Weppner, R. A. Huggins, *J. Electrochem. Soc.* **1977**, *124*, 1569.

[4] Y.-H. Zhu, X. Yang, D. Bao, X.-F. Bie, T. Sun, S. Wang, Y.-S. Jiang, X.-B. Zhang, J.-M. Yan, Q. Jiang, *Joule*, **2018**, *2*, 736.

[5] Z. Wang, W. Zhuo, J. Li, L. Ma, S. Tan, G. Zhang, H. Yin, W. Qin, H. Wang, L. Pan, A. Qin, W. Mai, *Nano Energy* **2022,** *98*, 107243.

[6] Y. Lin, J. Liu, L. Shi, N. Guo, Z. Sun, C. Geng, J. Jiang, Q. Zhuang, Y. Chen, Z. Ju, *J. Colloid Interface Sci.* **2022,** *623*, 1.

[7] C. Zhang, Y. Xu, M. Zhou, L. Liang, H. Dong, M. Wu, Y. Yang, Y. Lei, *Adv. Funct. Mater.* **2017,** *27*, 1604307.

[8] M. Qin, W. Ren, J. Meng, X. Wang, X. Yao, Y. Ke, Q. Li, L. Mai, *ACS Sustain. Chem. Eng.* **2019,** *7*, 11564.

[9] Y. Pei, C. Mu, H Li, F Li, J Chen, *ChemSusChem* **2018**, *11*, 1285.

[10] H. Kim, D. Seo, J. C. Kim, S. H. Bo, L. Liu, T. Shi, G. Ceder, *Adv. Mater.* **2017**, *29*, 1702480.

[11] B. Lin, X. Zhu, L. Fang, X. Liu, S. Li, T. Zhai, L. Xue, Q. Guo, J. Xu, H. Xia, *Adv. Mater***. 2019**, *31*, 1900060.

[12] J. Liao, Q. Hu, B. Che, X. Ding, F. Chen, C. Chen, *J. Mater. Chem. A*, **2019**, *7*, 15244.